



Effects of surface pretreatments and coating period on hydroxyapatite coating of Ti6Al4V alloy

T. Hacıoğlu¹ · Z. Evis^{1,2} · A. Tezcaner² · M. K. Aydınol^{1,3}

Received: 12 September 2018 / Revised: 5 March 2019 / Accepted: 5 May 2019 / Published online: 11 June 2019
© Australian Ceramic Society 2019

Abstract

In this study, Ti6Al4V plates were gone through three steps of pretreatment process (sandblasting + acid etching + preheating) followed by biomimetic coating of pure hydroxyapatites (HAp) on pretreated substrate. Pretreated substrates were examined by SEM, EDS, AFM, FTIR, and XRD; meanwhile, prepared coatings were examined by SEM, EDS, FTIR, XRD, XPS, scratch test, and in vitro cell studies (SaOS-2 cell line). Prepared coatings were also investigated in terms of antibacterial property by determining the survival of the *Staphylococcus epidermidis* on the surface. Structural analysis results of pretreated substrates proved that surface roughness increased proportionally as sandblasting, acid etching, and preheating process were performed. Successively, surface became more porous according to SEM images which were also supported by AFM results that indicate that Ra increased up to 953 nm values. EDS and FTIR spectra showed that functional groups were formed with the pretreatment procedure. Especially titanium salts were formed during acid etching process while preheating caused oxidation. XRD spectra revealed that as-received substrates mostly consisted of α -Ti, acid etching resulted in formation of TiH₂ structure and oxidation resulted to form rutile and anatase structure patterns. Pretreatment procedure had positive effect on biomimetic coatings according to the evaluation of structural, mechanical, and biological properties. SEM analysis revealed that HAp nucleation started 4 days after immersion and nucleation increased with the incubation time. EDS results indicated that maximum Ca/P ratio (1.48) was achieved by P14. FTIR, XRD, and XPS analysis proved the presence of hydroxyapatite on the substrate surface. The pretreatment procedure had significant influence on mechanical properties of the coatings resulting in increase of critical loads. P14 sample had the highest critical load. In terms of biological evaluation, P14 exhibited the highest cell proliferation and lowest bacterial adhesion. The highest stability and coherence of P14 coating was also confirmed by mechanical test results. Eventually, it was observed that pretreatment technique has great effect on surface properties. In addition, 14 days immersion period was found to be optimum along the investigated immersion times.

Keywords Sand blasting · Acid etching · Preheating · Hydroxyapatite · Ti6Al4V

Introduction

Ti and its alloys are commonly preferred implant materials for hard tissue applications. According to a research conducted in

2006, more than 4.4 million people had an internal fixation device and over 1.3 million people possess an artificial joint [1]. Common problems associated with patients who had revision surgeries are instability, aseptic loosening, infection, wear, osteolysis, ingrowth failure, and periprosthetic fracture [2, 3]. Compared to other traditional metallic biomaterials, Ti alloys possess lower modulus, better biocompatibility, and corrosion resistance [4]. The main drawback for utilizing Ti-based biomaterials is its necessity to improve its biocompatibility. It is known that surface pretreatment techniques are an effective way to obtain microporous structures which improve the bioactivity and osseointegration of Ti implants. On the other hand, surface treatments are not adequate to achieve a decent osseointegration level. One of the solutions to overcome poor osseointegration of metallic biomaterial is to modify Ti surface and coat the surface with hydroxyapatite (HAp,

Available Online at: www.austceram.com/ACS-Journal

✉ Z. Evis
evis@metu.edu.tr

- ¹ Department of Micro and Nano Technology, Middle East Technical University, Ankara, Turkey
- ² Department of Engineering Sciences, Middle East Technical University, Ankara, Turkey
- ³ Department of Metallurgical and Materials Engineering, Middle East Technical University, Ankara, Turkey

$\text{Ca}_{10}(\text{PO}_4)_6(\text{OH})_2$) which has very similar composition to natural human bone [5]. There are several HAp coating techniques such as biomimetic coating, plasma spraying, sol-gel technique, and some other methods. Among these techniques, biomimetic coating enables the use of low processing temperatures and coating complex shapes. On the other hand, it also has some disadvantages, such as difficulty in production of crack-free coatings and non-uniform coating thickness.

Fujibayashi et al. focused on deforming Ti surface via oxidation technique and examined the characteristics of porous Ti substrate [6]. Since then, researchers gave attention to the modification of Ti surface prior to coating process. Certain pretreatment techniques for instance alkalization, acid etching, sand blasting, UV exposure, grinding, polishing, and pre-heating are commonly studied to obtain porous substrate surface. On the other hand, it is rare to combine several pretreatment techniques respectively [7, 8]. Xu et al. studied the effect of surface modification for Ti substrate earlier on HAp coating via sandblasting and acid etching treatments. The researchers demonstrated that sandblasted-acid-etched Ti substrate was converted into a more bioactive surface after HAp coating, hereby claiming that modified Ti substrate with the HAp coating can promote bone formation around implants and increase the survival rate of implants for patients with poor bone quality [5]. Liu et al. described a coating process using a chemical method to prepare calcium carbonate coatings onto sandblasted and acid-etched Ti substrate and smooth Ti as control. They have pointed out that optimal biological response was observed on calcium carbonated coatings on sandblasted-acid-etched substrate [9]. As described in the studies, prior to the HAp deposition, sandblasting and acid etching treatments have great effect on the surface properties of Ti-based substrate, likewise, preheating is also very crucial for the surface properties, it can promote the crystallization and the formation of film-like deposits [10]. Kokubo and Yamaguchi reviewed about a number of researches that sought out the influence of acid etching and preheating ahead of coating in order to promote osteointegration by generating a rough substrate surface. Researchers recommended that acid-treated Ti metal implants should be subsequently exposed to a heat treatment to ensure stable fixation due to its bonding to the bone [7]. An et al. studied the pretreatment effect from different points of view, they conceived that as a pretreatment technique acid etching followed by pre-heating step increased roughness and promoted mechanical and biological properties compared to other pretreatment techniques [11]. In some studies, researchers exhort further treatment instead of two-step pretreatments. For instance, Chen et al. investigated thoroughly osseointegration of sandblasted/acid-etched (SLA) and anchored calcium phosphate (CaP) implants in vivo. They found out that the osseointegration performance of the SLA with anchored CaP on the implant surface was much better than that of the SLA-only group in terms of contact with the

implant percentage [12]. Deng et al. reported a method for combining sandblasting, acid etching, and micro-arc oxidation treatments to optimize titanium implant surfaces. As a result, the combination of sandblasting, acid etching, and micro-arc oxidation techniques had enhanced the titanium surface morphology and increased the roughness parameters which provided a better surface for stem cell differentiation and osseointegration [13]. Consequently, it was hypothesized that combining several pretreatment techniques would result in better substrate surface prior to HAp coating.

In this study, the effect of pretreatment steps on Ti6Al4V substrate and the properties of biomimetic HAp coatings on the pretreated substrates were investigated. Pretreatment process was conducted to obtain rougher and proper surface in order to achieve better HAp deposition onto the substrate surface. It should be noted that this work is the first reported attempt to perform the three-step pretreatment procedure (sandblasting, acid etching, and preheating) of the Ti6Al4V substrate prior to biomimetic deposition of HAp. Using three-step pretreatment technique promoted the deposition of HAp on the surface of Ti6Al4V. Furthermore, the influence of biomimetic coating period was also studied. Pretreated substrates were examined by SEM, EDS, AFM, FTIR and XRD; meanwhile, HAp coatings were examined by SEM, EDS, FTIR, XRD, XPS, scratch test, in vitro cell studies, and antibacterial survival assessment with *Staphylococcus epidermidis*.

Methods and procedures Bulk Ti6Al4V (Grade 5) was used as a precursor and the bulk metallic sample was cut into small pieces with $10 \times 10 \times 1.2 \text{ mm}^3$ dimensions via water jet. Curtailed pieces of Ti6Al4V alloy were firstly gone through sandblasting (S), secondly H_2SO_4 (%48 wt.) (Merck KGaA, Darmstadt, Germany) acid etching (A), and finally, heating (P) at $600 \text{ }^\circ\text{C}$ for 1 h treatments. Schematic representation of the pretreatment procedure is shown in Fig. 1. To be more precise, sandblasting was performed for 3 min via sandblasting gun or sandblasting drum. In both mediators, SiO_2 particles used were of spherical form with an average diameter of 250–300 μm . H_2SO_4 (%48 wt., 1 M) acid etching was performed at $200 \text{ }^\circ\text{C}$ for 30 min by using a heater [14]. Acid etching process was followed by washing the plates in distilled water and drying them in a desiccator at room temperature. Preheating process was carried out in a dry furnace at $600 \text{ }^\circ\text{C}$ for 1 h. After preheating, samples were kept in a furnace in overnight period for cooling [15].

SBF solutions were prepared by using analytical grade NaCl, NaHCO_3 , KCl, $\text{K}_2\text{HPO}_4 \cdot 3\text{H}_2\text{O}$, $\text{MgCl}_2 \cdot 6\text{H}_2\text{O}$, CaCl₂, and Na_2SO_4 (Merck KGaA, Darmstadt, Germany) according to Kokubo and Takadama technique [16]. The ionic concentrations of the blood plasma and pure SBF solutions are shown in Table 1. The salts were dissolved in 1000 ml of distilled water at $37 \text{ }^\circ\text{C}$ under constant vigorous stirring. The final pH of the solutions was adjusted to 7.40 at $37 \text{ }^\circ\text{C}$ by adding 1 M

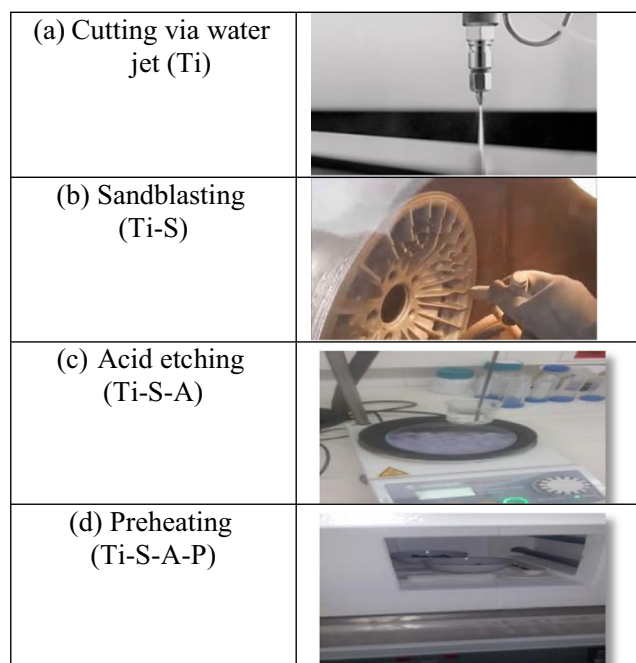


Fig. 1 Schematic representation of pretreatment procedure. **a** Ti, **b** Ti-S, **c** Ti-S-A, **d** Ti-S-A-P

HCl solution (Merck KGaA, Darmstadt, Germany) and TRIS buffer (Merck KGaA, Darmstadt, Germany), alternatingly.

Afterwards, pretreated plates were immersed into pure 1.5× SBF solution for 4, 7, 14, and 21 days in order to achieve biomimetic deposition of apatite compounds which are calcium ortho phosphates with a formula of $\text{Ca}_{10}(\text{PO}_4)_6(\text{OH})_2$ with small amount of impurities. During the immersion period, the solutions were discarded and replaced with freshly prepared solutions once in every 2 days. Temperature was kept constant at 37 °C by using a shaking water bath. Prepared coatings were coded according to their coating period.

The surface topography and roughness of abraded and pretreated samples were examined with an atomic force microscope (Veeco MultiMode V model, AFM). Roughness parameters were evaluated in terms of R_a , R_z , and R_q . The surface morphology of the abraded, pretreated, biomimetically

Table 1 Ionic concentrations of 1.5× blood plasma and pure 1.5× SBF-coated samples

Ion	1.5× blood plasma (mM) [12]	Pure 1.5× SBF (mM) [16]
Na^+	213.00	214.09
K^+	7.50	7.56
Mg^{2+}	2.25	2.29
Ca^{2+}	3.75	3.95
Cl^-	154.50	223.24
HCO_3^-	40.50	6.34
HPO_4^{2-}	1.50	1.52
SO_4^{2-}	0.75	0.76

coated, and cell-seeded plates was observed with a scanning electron microscope (QUANTA 400F Field Emission SEM). In addition, elemental composition of the coatings was analyzed by using the energy dispersive X-ray spectroscopy (JXA-8230 EDS) set-up. For FTIR analysis, a spectrometer (Perkin Elmer 400, Germany) was used and the samples were examined in the mid-infrared (MIR) range ($4000\text{--}400\text{ cm}^{-1}$). XRD analysis was performed with a diffractometer (Rigaku Ultima-IV, Japan) with $\text{Cu-K}\alpha$ radiation at 40 kV and 30 mA. A pretreated plate without a coating was introduced as blank and the pattern of substrate itself was subtracted from XRD data of the coated samples. XRD data were also assessed by the Rietveld method. X-ray photoelectron spectroscopy (XPS) was performed by using a PHI 5000 VersaProbe. X-ray photoelectron spectroscopy is a technique for analyzing the surface chemistry of a material. XPS can measure the elemental composition, empirical formula, chemical state, and electronic state of the elements within a material.

Scratch tests were run with a scanning scratch tester (Shimadzu SST-W101, Japan). The scratch test was used to evaluate the adhesion of the HAp coating to the underlying substrate. The scratch tests were conducted using a scratch tester with a linear and progressive load, with the following test parameters: scratch pre load of 0.05 N, load speed of 0.47 N/min, and end load of 1 N. The scratch length was 4 mm. The scratch test consisted of generating scratches using a Rockwell diamond tip with 100 μm radius (serial number I-128) maintained at a constant speed over the surface under different test loadings. Series of scratch tests were performed with normal loads on a coating to obtain a load where the coating exhibited failure. Each scratch was evaluated by the use of an optical microscope for failure. The load at which such failure of the coating occurs is termed as the critical load (L_c).

Osteogenic-committed cell line Saos-2 (CRL-7939, ATCC, Manassas, USA) was used in cell culture studies. They were cultured in complete growth medium (Dulbecco’s Modified Eagle Medium (DMEM, Biowest, Nuaille, France)) supplemented with 10% Fetal Bovine Serum (FBS) (Biowest, Nuaille, France) and 1% penicillin/streptomycin solution (Biowest, Nuaille, France) at 37 °C in a humidified incubator with 5% CO_2 . To evaluate cytocompatibility of coated substrates, coated Ti6Al4V plates were sterilized in a dry-heat furnace at 200 °C for 2 h. In order to prevent spontaneous crack formation on the HAp coatings, the samples were left to cool slowly during overnight in the furnace. SaOS-2 cells were then seeded onto coated samples at a density of 50,000 cells/sample and Alamar Blue test was conducted at predetermined time periods (days 1, 3, and 7) to determine the viability of the cells in terms of percent reduction. The Alamar Blue assay is based on the detection of cell metabolic activity, which determines the chemical reduction of the Alamar Blue (Thermo Fisher Scientific, MA, USA) dye, thus

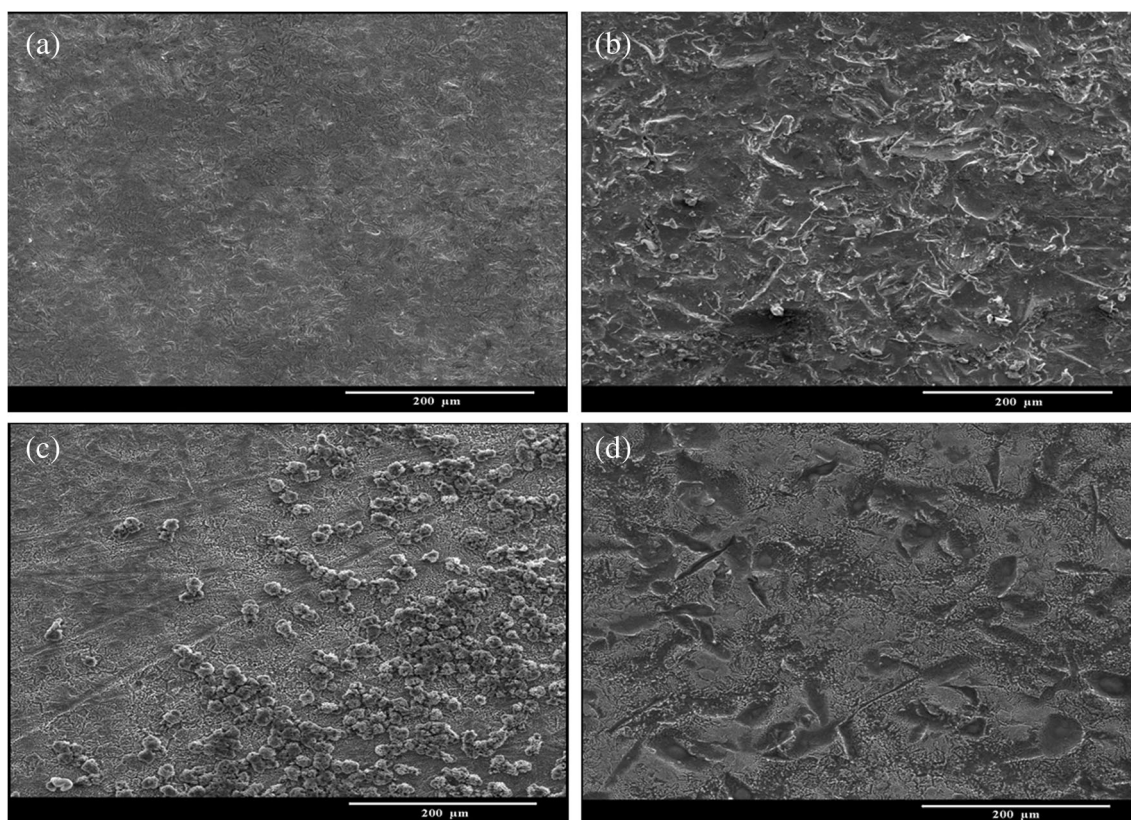


Fig. 2 SEM images of **a** Ti, **b** Ti-S, **c** Ti-S-A, and **d** Ti-S-A-P ($\times 500$)

producing a color change from blue to red. Alamar Blue solution ((Dulbecco's Modified Eagle Medium (DMEM Gibco, Biowest, Nuaille, France) supplemented with 10% Fetal Bovine Serum (FBS) (Biowest, Nuaille, France), 10% Alamar Blue, and 1% penicillin/streptomycin solution (Biowest, Nuaille, France)) was used for absorbance reading. Alamar Blue solution was replaced with growth medium and Alamar Blue-added wells were incubated for at least 4 h at 37 °C in a humidified incubator with 5% CO₂. The absorbance at 600 nm was subtracted from the absorbance at 570 nm for each individual well. Control negative samples (c⁻) were composed of medium and Alamar Blue (no cells, no plates). On the other hand, positive control samples (c⁺) were cells seeded on culture plates. The absorbance is a direct measure of cellular viability since it is a result of the ability of the cells to reduce the active ingredient. Increase in percent reduction can be interpreted as cell proliferation. To calculate, percentage of reduction Eq. (1) was used due to U.S. Patent No. 5501959:

$$\text{Reduc.(\%)} = \frac{(117216 \times \text{Sample at 570 nm}) - (80586 \times \text{Sample at 600 nm})}{(155677 \times (\text{c}^-) \text{ at 600 nm}) - (14652 \times (\text{c}^-) \text{ at 570 nm})} \times 100 \quad (1)$$

Inductively coupled plasma/mass spectrophotometry (ICP/MS) analysis was performed by using a Thermo Electron

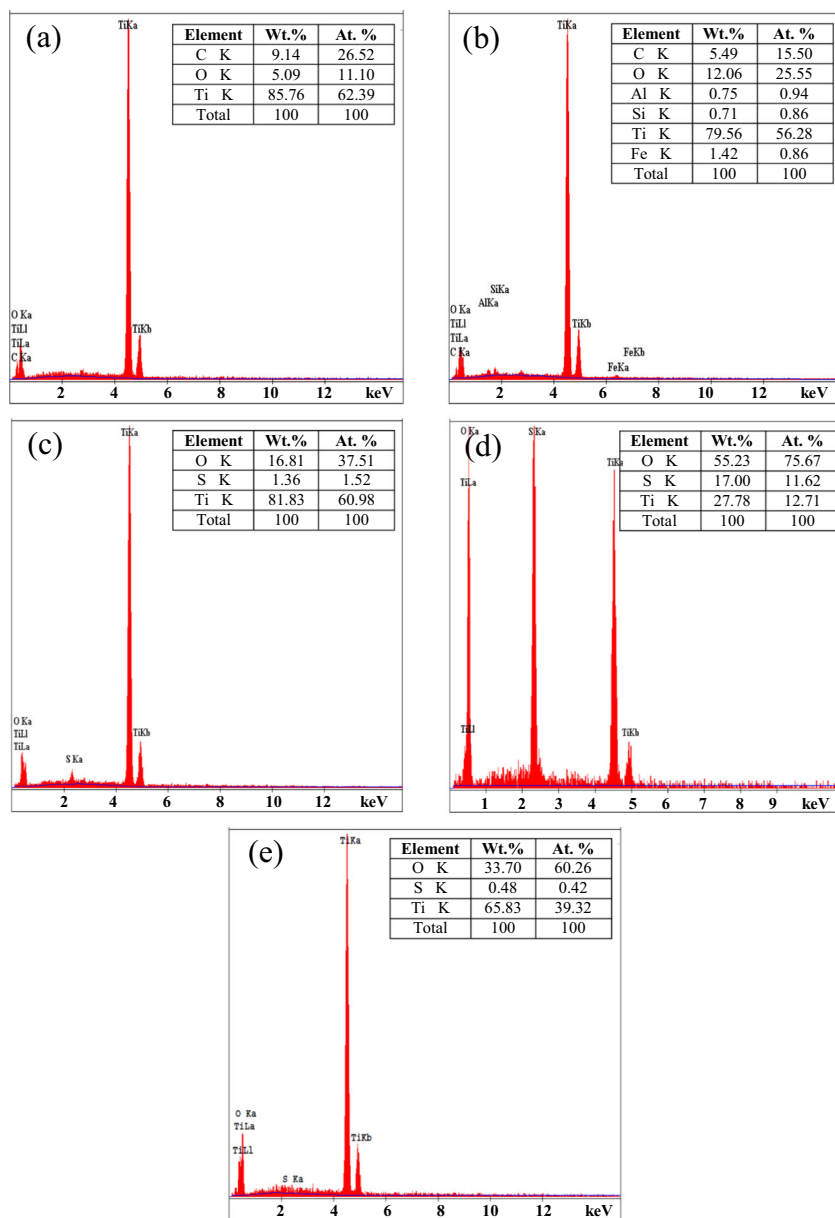
X7 device (Thermo Fisher Scientific, USA) in order to determine Ca and P amounts in cell culture media.

Prior to the antibacterial test, *Staphylococcus epidermidis* bacteria (ATCC 12228, Manassas, USA) were cultured on nutrient agar plates at 37 °C. A 10⁶ colony-forming unit (CFU) mL⁻¹ bacterial suspension was prepared using a 1:500 diluted nutrient broth (NB). Coated Ti6Al4V plates were sterilized in a dry-heat furnace at 200 °C for 2 h. The antibacterial tests were performed with three replicates from each group. A 50-μL aliquot of the bacterial suspension was dispensed into the sterilized specimens and covered with a 15 × 15 mm cover glass. The specimens were subsequently placed into an incubator set at 37 °C with 95% humidity and incubated for 4 h. After the incubation period, the samples were washed with 5 ml of PBS solution and subsequently cultivated on the surface of a nutrient agar plate (100 μL). The colonies formed on the plate surface were counted and the results were obtained in colony forming units per milliliter [1, 17].

Results and discussion

SEM images of as received and pretreated plates are shown in Fig. 2. As seen from Fig. 2(a), Ti plate surface was quite smooth. In order to enhance the mechanical interlock between

Fig. 3 EDS spectra of **a** Ti, **b** Ti-S, **c** Ti-S-A pore side, **d** Ti-S-A crystal side, and **e** Ti-S-A-P



the coating particles and the metal surface, abrading process was applied to the Ti6Al4V plates. Figure 2(b) shows that the surface of sandblasted plate was deformed and became rougher. To remove the sand particles observed on Ti-S, acid etchant was implemented on the sandblasted samples. Figure 2(c) revealed that the salt crystal formation occurred during acid etching. During acid etching process, substrate material became rougher and much more porous. Meanwhile, crystal titanium salts were formed on the surface. Acid etching process was followed by the preheating step. Figure 2(d) shows SEM images of Ti-S-A-P. The plate surface was oxidized by preheating process. It may be arisen from the grain boundary shrinkage and oxidation. As explained in the introduction part, the preheating step was expected to stabilize the coating on the surface.

EDS spectra of as-received and pretreated plates are demonstrated in Fig. 3. EDS spectrum seen in Fig. 3(a) proved that Ti alloy used as a substrate is mainly composed of TiK α . Not surprisingly, EDS spectrum in Fig. 3(b) supported the presence of sand particles on the surface, Si and Al peaks were observed. EDS spectra shown in Fig. 3(c) and (d) showed the presence of titanium salt crystals formed during acid etching. EDS spectra revealed that titanium salts were composed of sulfur (S), oxygen (O), and titanium. According to this information reaction (2) occurred and ultimately the crystal salts formed were TiSO₄ [14].

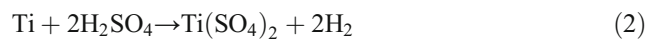
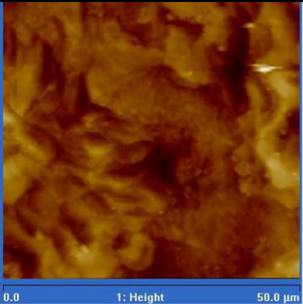
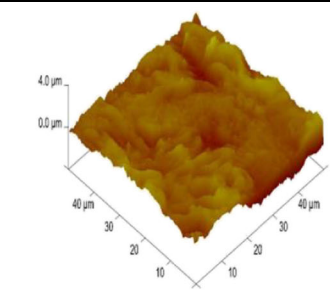
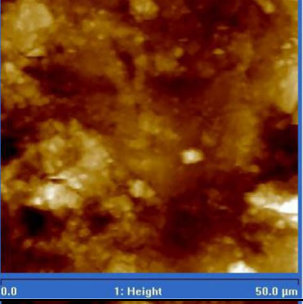
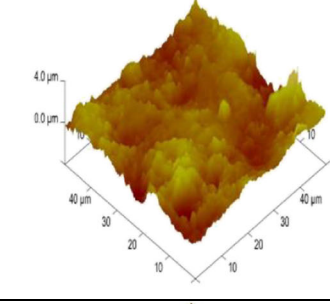
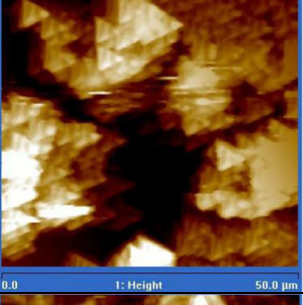
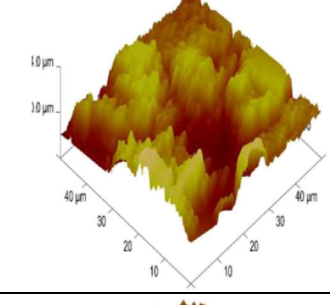
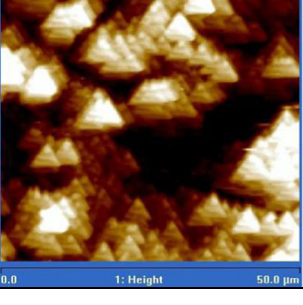
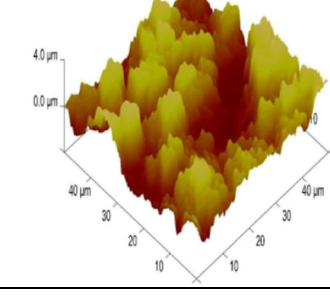


Table 2 Roughness and topography of Ti, Ti-S, Ti-S-A, and Ti-S-A-P

Sample	Roughness (nm)			2D image	3D image
	R _a	R _q	R _z		
Ti	260	337	228		
Ti-S	397	507	196		
Ti-S-A	848	1057	747		
Ti-S-A-P	953	1148	973		

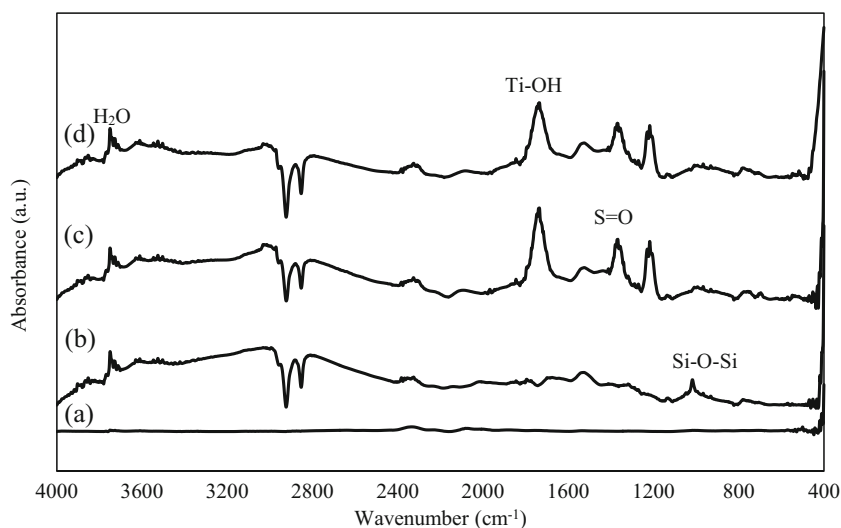
According to Ban et al., a 30-min period is optimum for acid etching process. For a period of 30 min, the grain boundaries were obvious and the crystal grains were distinguishable. The grain surface showed micro-porosities owing to the formation of micro-pits smaller than 1 μm in diameter [14]. Moreover, EDS spectra of Ti-S-A (Fig. 3(c) and (d)) verified that sand particles were removed by acid etching process (Si and Al peaks were lost). As expected, after the preheating step, sulfur content decreased while Ti content increased as observed in Fig. 3(e).

Surface roughness increased due to pretreating routine. Roughness parameters and topographies are shown in

Table 2. Ra value provides average roughness information. According to Ra values and the topographic images, it is seen that the surface became rougher and porous collaterally with the pretreatment procedure. As-received titanium alloy (Ti) had the lowest roughness degree (about 180–300 nm) which was similar to a literature work [18]. Sandblasting process evoked an increment in small pits and decrement in large pits by smoothing them [19].

It was observed that acid etching process (Ti-S-A) caused enormous deformation on the surface, meanwhile (111) face-centered cubic (fcc) planes were also clearly seen in 2D image [20]. Similar to literature work, combined process of

Fig. 4 FTIR spectrum of **a** Ti, **b** Ti-S, **c** Ti-S-A, and **d** Ti-S-A-P



sandblasting and acid etching increased the surface roughness [9, 21]. Finally, preheating step (Ti-S-A-P) caused surface oxidation and increased roughness up to 953 nm, thus still (111) fcc plates dominated the surface [22].

FTIR spectra of untreated and pretreated plates are represented in Fig. 4. Ti plate had no detectable functional group as shown in the spectrum. The characteristic bands observed in Ti-S samples belong to Si-O-Si stretching mode at 1083–1089 cm^{-1} [23]. Bands observed in Ti-S-A and Ti-S-A-P samples at 1172–1214 cm^{-1} and 1443–1446 cm^{-1} were attributed to S=O stretching [24]. Ti-OH stretching mode was observed at 1637–1641 cm^{-1} [25]. Furthermore, the weak bands at 3500–3700 cm^{-1} were attributed to moisture [26]. In most cases, a weak peak around 2349 cm^{-1} was caused by the CO_2 presence in the beam (poor background correction). In samples except Ti plate, a weak peak around 1600 cm^{-1} was observed due to O-H stretching [27]. Downward peaks observed were the result of inadequate background correction.

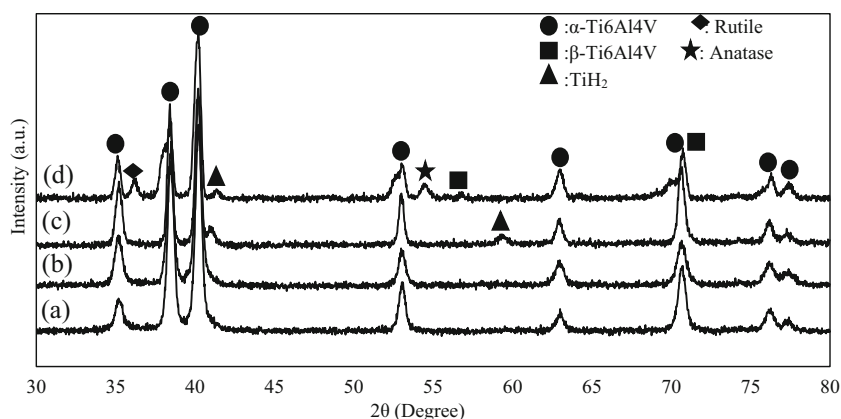
The XRD patterns of the as-received Ti6Al4V plate and pretreated plates are presented in Fig. 5. Since there is no JCPDS standard for Ti6Al4V, fitting results of the hexagonal α -Ti (JCPDS file #44–1294) and the cubic β -Ti (JCPDS file

#44–1288) were used for labeling. As observed from Fig. 5, all plates (Ti, Ti-S, Ti-S-A, and Ti-S-A-P) showed mainly α -Ti peaks though β -Ti peaks were weaker. Both rutile and anatase peaks were present in preheated plates (Ti-S-A-P) due to high temperature oxidation [28]. Furthermore, TiH_2 peaks (ICDD # 09–037) were present in acid-etched (Ti-S-A) and preheated (Ti-S-A-P) plates. The intensity of TiH_2 was the sum of the intensities of the (110) shoulder peak at 40.9° and the (200) peak at 59.6° for 2θ . Though TiH_2 (200) peak was lost after preheating step. This suggests that secondary reaction occurs as given in Eq. 3 [14, 15].



Substantial reason for investigating the pretreatment steps was to find out the procedure that enables to obtain the most deformed (maximum roughness) and stable surface prior to HAp deposition. According to the analysis results of pretreated samples, it seems that the roughest and stable surface was pertained to Ti-S-A-P. This hypothesis was also corroborated by the comparison of Ti, Ti-S, Ti-S-A, and Ti-S-A-P

Fig. 5 XRD patterns of **a** Ti, **b** Ti-S, **c** Ti-S-A, and **d** Ti-S-A-P



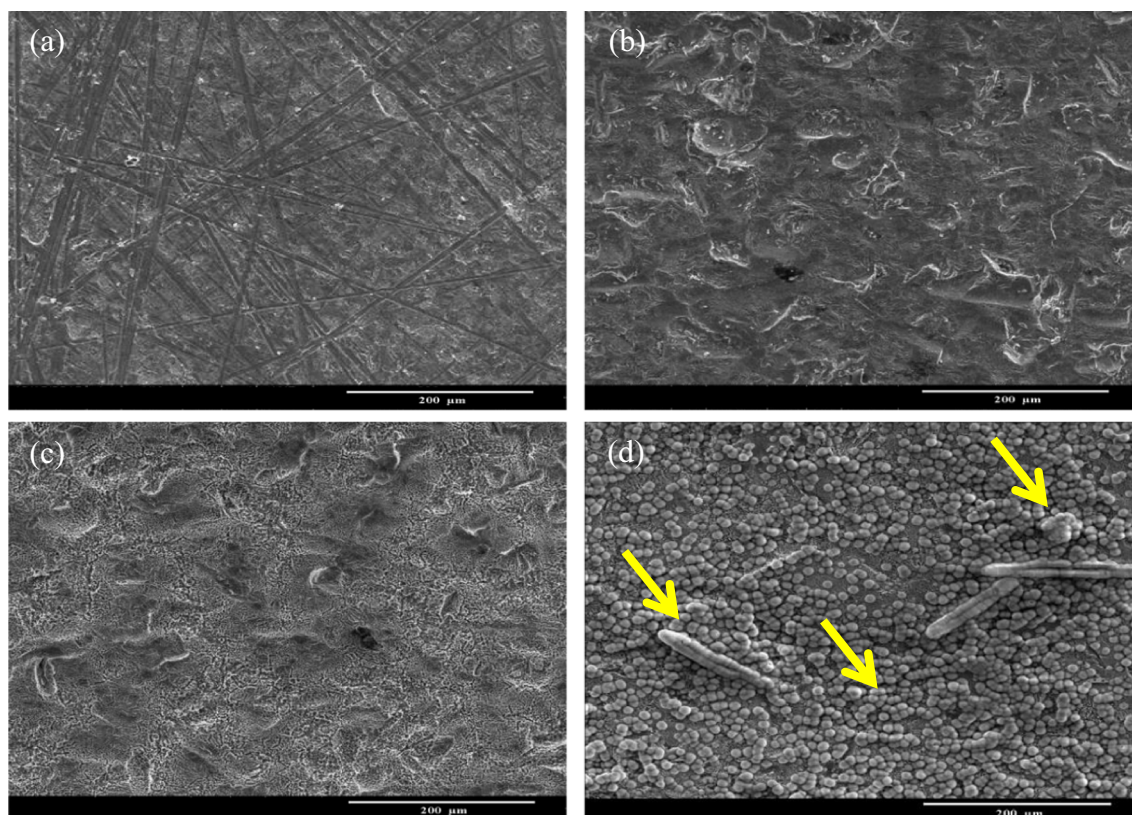


Fig. 6 SEM images of **a** Ti, **b** Ti-S, **c** Ti-S-A, and **d** Ti-S-A-P samples soaked in 1.5× SBF for 21 days at 37 °C (500×). Arrows indicate HAp particles precipitated on the surface

(also named as P21) samples soaked in pure 1.5× SBF for 21 days' period. Figure 6 and Table 3 give SEM and EDS results of different samples soaked in 1.5× SBF solution for 21 days. Maximum soaking time (21 days) was implemented to different substrates in order to evaluate the level of HAp deposition on the surface. Eventually, HAp particle deposition on the substrates except Ti-S-A-P was not accomplished. Hence, Ti-S-A-P pretreatment procedure was selected as the optimum technique. In addition, HAp particles which were deposited on Ti-S-A-P surface (Fig. 6(d) shown with arrows) were in globular shape and some of them were nucleated vertically.

Table 3 EDS results of pretreated samples soaked in 1.5× SBF for 21 days at 37 °C

Sample	Element	wt%	at %
Ti	Ti	100	100
Ti-S	Ti	100	100
Ti-S-A	Ti	100	100
Ti-S-A-P	O	50.66	68.45
	Na	4.45	4.18
	Mg	1.47	1.31
	P	16.59	11.58
	Ca	26.83	14.47

SEM images of Ti-S-A-P plates after soaking in pure 1.5× SBF for a period of 4 days (P4), 7 days (P7), 14 days (P14), and 21 days (P21) are shown in Fig. 7. As observed from Fig. 7, HAp nucleation started in 4 days' period. HAp particles were present in globular form. HAp precipitation was drastically improved with increasing the incubation period in SBF. The surface of the Ti6Al4V plates was entirely covered with numerous, spherical and granular CaP precipitates after 7 days in 1.5× SBF. For 14 days soaking period, HAp crystals were vertically nucleated all over the surface while for 21 days soaking period HAp particles almost fully covered the surface and horizontal growth occurred. SEM images given in Fig. 7 showed that the CaP layer was grown steadily as a result of this process. One of the most important techniques used for validating HAp presence (due to Ca and P composition) is EDS analysis. Ca/P molar ratios of the coatings obtained from the 1.5× SBF calculated were as follows 1.44 on day 4, 1.47 on day 7, 1.48 on day 14, and 1.25 on day 21. EDS results are obtained from few micrometers area on the substrate's surface, as a result of this fact, sudden drop in Ca/P ratio can be observed. It should be noted that in case of 14 days coating period, Ca/P ratio was almost the same with the human bone which is 1.5 [29]. Figure 8 represents FTIR spectra of Ti-S-A-P plates that were incubated in pure SBF for different immersion times. Similar functional groups were detected in all cases, though the peak intensities differed. The peak of

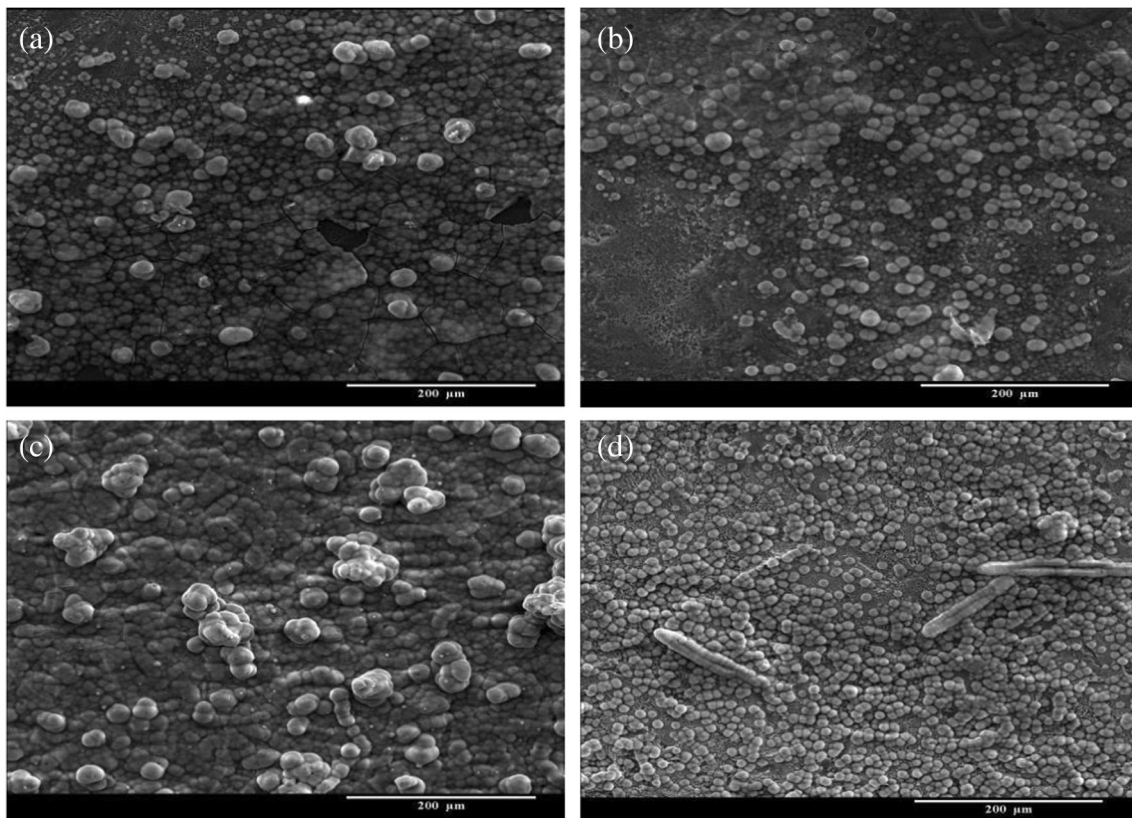


Fig. 7 SEM images of **a** P4, **b** P7, **c** P14, and **d** P21 (500 \times) samples

$\nu_4\text{PO}_4^{3-}$ bending was observed at around 560 cm^{-1} generated from phosphate ion. The shoulder of this bending was assigned to $\nu_1\text{CO}_3^{2-}$ stretching. The bands around 1020 cm^{-1} were due to $\nu_3\text{PO}_4^{3-}$ stretching mode while the bands around 1400 cm^{-1} were attributed to $\nu_1\text{CO}_3^{2-}$ and $\nu_3\text{CO}_3^{2-}$ stretching mode of carbonate [30–33]. All characteristic bands of HAp were obtained after each coating period [34]. The difference in peak intensities of the P7 sample was related to additional TCP ($\text{Ca}_3(\text{PO}_4)_2$) formation at this soaking period.

Anatase (TiO_2), rutile (TiO_2), TCP, and HAp phases were detected in the coatings (Fig. 9). All coatings exhibited standard

HAp XRD peaks. As the immersion time increased, XRD peaks sharpened due to the increase in coating thickness and crystallization. HAp crystallizes in hexagonal crystal form. It should also be noted that preferred orientation of HAp growth occurred on surfaces resulted in modified intensity of HAp peaks when compared to the standard peaks. As seen from Fig. 9, P7 has higher peak intensity at around 25° and 32° compared to others due to additional TCP formation. This additional TCP formation at 7 days' period was also compatible with FTIR results (more PO_4^{3-} groups were present in P7 sample). As expected, Ti phase intensity decreased as the coating period and HAp deposition

Fig. 8 FTIR spectra of **a** P4, **b** P7, **c** P14, and **d** P21

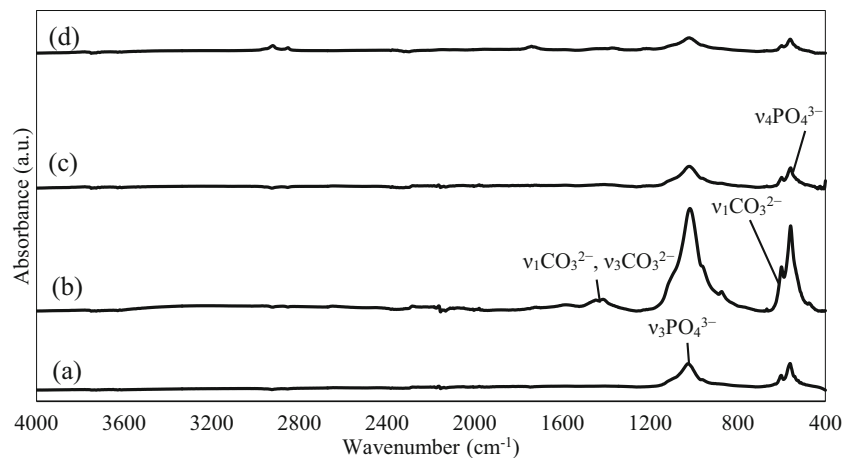
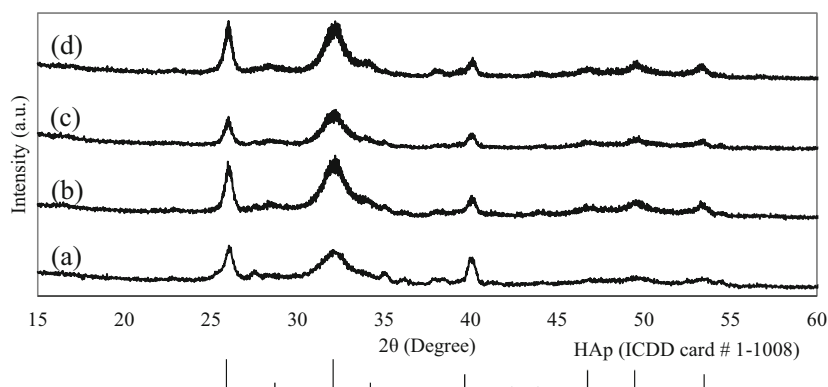


Fig. 9 XRD patterns of **a** P4, **b** P7, **c** P14, and **d** P21 samples



increased [33, 35]. The results of Rietveld analysis obtained from XRD data provided the mean lattice parameters that were approximately $a = 9.4492 \text{ \AA}$ and $c = 6.8739 \text{ \AA}$.

The calculated lattice parameters were consistent with HAp cif. file (code:1617565) where $a = 9.4232 \text{ \AA}$ and $c = 6.8833 \text{ \AA}$. Slight difference in parameter values was negligible. Similar to this study, Sumathi & Buvanewari determined the lattice parameters of the compound by least square fitting of high-angle lines. The unit cell parameters were: $a = 9.4122 \text{ \AA}$, $c = 6.922 \text{ \AA}$ and the unit cell volume was 530.9 \AA^3 [36].

XPS analysis of P14 was performed. XPS technique provided atomic ratios. From the atomic ratios, chemical composition of the surface coating can be determined. Spectroscopy technique does not provide reliable oxygen content. Moreover, it does not allow calculating the amount of hydrogen. According to the spectroscopy results, $\text{Ca}_9(\text{PO}_4)_7.2(\text{OH})_x$ compound formula was obtained as a coating material.

In order to assess mechanical properties, scratch tests were carried out to find out the adhesion of coating on the substrate surface by means of critical load. Critical load is the load where the coatings are detached from surface. Table 4 showed the critical loads of prepared $1.5\times$ SBF coatings. As seen from the table, all of the critical loads were above 100 mN. P14 exhibited the highest critical load. It is known that pretreatment techniques can improve mechanical properties by deforming the metal surface and leading to increase in the level of surface roughness [37, 38]. Compared to studies in literature, critical loads were quite high, for instance alkali-pretreated and selenium-doped SBF-coated Ti6Al4V plates exhibited much lower critical loads (about 70 mN) [39]. To sum up, pretreatment techniques modify the surface and make

a way for obtaining rougher surface which enables higher degree of HAp deposition during coating process. In some cases like three-step pretreatment technique (Ti-S-A-P) conducted in this study, pretreatment technique can also lead to attain stronger mechanical bonding between HAp coating and the metallic substrate.

Cytotoxicity and antibacterial properties of the coatings were evaluated to determine biological properties. The reduction percentage of SaOS-2 cells seeded on coated sample coatings was shown in Fig. 10. Percentage of reduction increase is directly related to development of cell proliferation. Percentage of reduction increases as cell mitochondrial activity increase which is related to the number of cells containing mitochondria. There are some important results obtained from Fig. 10. First of all, it was determined that P7 had the best initial cell attachment 1 day after cell seeding. According to day 1 readings, fewer cells were attached to the surfaces of P14 and P21 samples. Considering the whole cell seeding proses, P14 showed maximum increment in percentage of reduction and cell proliferation. In all coating periods, cell proliferation increased, particularly P14 coating's cell proliferation developed greatly compare to other coatings. As expected, surface pretreatment procedure had beneficial effects on cell proliferation with moderately rough surfaces [40, 41]. The results were consistent with several studies which demonstrated that rough titanium surfaces increase the cell attachment as compared to smooth ones [9]. Effect of immersion period was also studied by some other researchers. Avci et al. studied similar preparation and cytotoxic assessment technique, as a result they claimed that approximately 2 weeks immersion period was the optimum period due to high cell proliferation on these types of surfaces [30]. Alternatively, Yilmaz et al. also performed similar production and cytotoxic assessment method, ultimately 14 days coated samples had lower cell viability compared to 7 days coated samples. The researchers suggested that the coating homogeneity and coverage was an important factor in terms of cell proliferation and the deposited apatite may had been lost with the attached cells on the coatings obtained at the 14th day during medium renewal stage [39].

Table 4 Critical loads of Ti-S-A-P plates after soaking in pure $1.5\times$ SBF for 7, 14, and 21 days

Sample	Critical load (mN)
P7	100 ± 1.17
P14	270 ± 3.15
P21	250 ± 3.01

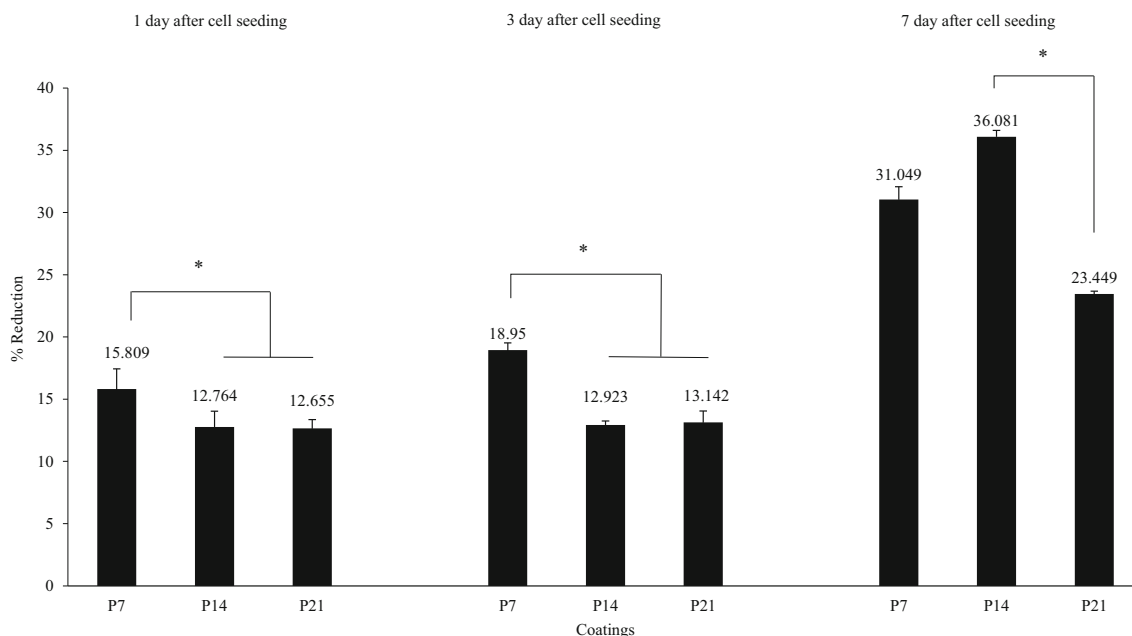


Fig. 10 Percentage of reduction of cells seeded on pure SBF coated samples. The error bars represent the standard error. Asterisks indicate differences of statistical significance ($*p < 0.05$) within the groups determined by the ANOVA test

According to Ca ions detected from the ICP/MS results (Table 5) of mediums collected at renewal periods, P21 was expected to obtain higher percentage of reduction than P14. The amount of Ca ion indicates the level of cell proliferation and HAp deposition. These unexpected drops in cell reduction percentages of P21 sample might be due to loss of deposited apatite with the attached cells during medium renewal stage. On the other hand, cell culture results were quite convenient with the results of mechanical analysis. P14 showed the most coherent and stable HAp coating according to its higher critical load value. Unsurprisingly, sample P21 had similar but slightly lower critical load compared to sample P14.

Antibacterial activity results of Ti-S-A-P plates after soaking in pure $1.5 \times$ SBF are shown in Fig. 11. Results were obtained in colony forming unit (cfu) term which represents the number of bacterial colonies reproduced on the substrate;

hence, it should be better to obtain less cfu on the sample. Results indicated that fewer bacteria adhered to P14 coating compared to P7 and P21 coatings. It should also be mentioned that in terms of bacterial colony forming unit, there was no significant difference between P7 and P14 samples. Antibacterial test results were compatible with cell culture and mechanical test results.

P14 coating was the most cytotoxic and coherent sample among other prepared coatings. These superior properties of P14 were also supported by antibacterial test; fewer bacteria were attached to the P14’s surface as a matter of homogenous and coherent HAp coating. Yilmaz et al. studied similar biomimetic coating technique and they also found out very

Table 5 ICP/MS results of mediums collected during cell culture

Medium collection period after cell seeding	Sample	Ca (mg/L)	P (mg/L)
1	P7	34	34
	P14	20.9	27.7
	P21	50	26.1
3	P7	55	25.1
	P14	44	18.4
	P21	61	21.9
7	P7	81	39
	P14	94	35
	P21	90	30.9

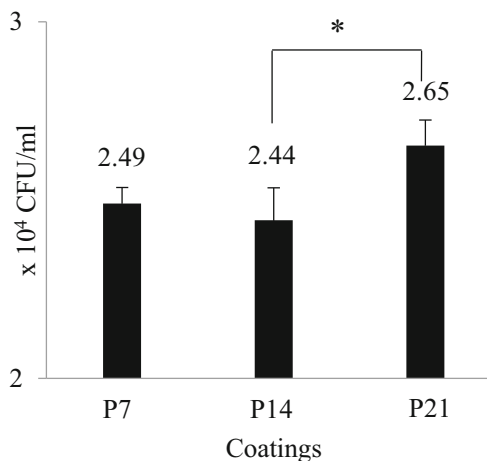


Fig. 11 Colony forming units per milliliter of coatings. The error bars represent the standard error. Asterisks indicate differences of statistical significance ($*p < 0.05$) within the groups determined by the ANOVA test

similar antibacterial test results for pure HAp coatings. They presented comparison between 7 and 14 days HAp-coated samples and resulted that slightly less bacteria were attached to the surface of 14 days' coatings [39]. From another point of view, the antibacterial property of pure HAp coatings can be enhanced by the addition of some antibacterial ions such as Ag^+ , Cu^{2+} , and Zn^{3+} according to literature works [42].

Conclusion

In this study, as-received Ti substrate was exposed to three-step (Ti-S, Ti-S-A, Ti-S-A-P) pretreatment procedure and concerning analyses were performed. Besides all pretreated samples were also compared after the immersion in pure $1.5\times$ SBF for 21 days' period to evaluate the level of HAp deposition on their surface. Ti-S-A-P had the maximum roughness and the most stabilized surface which makes it optimum substrate for coating process. After the selection of ideal substrate surface, biomimetic coating was performed for 4, 7, 14, and 21 days period. The SEM studies indicated that HAp nucleation started on the fourth day of immersion and increased with the incubation time. The results of structural analysis revealed the presence of HAp in all coating periods. In addition, mechanical tests and biological evaluations showed that P14 was the most coherent, osseointegrative, and antibacterial sample. Further in vivo studies with animal models are necessary for a better understanding of the osteointegration properties of HAp coated on modified titanium surface.

References

- Chen, W., Liu, Y., Courtney, H.S., Bettenga, M., Agrawal, C.M., Bumgardner, J.D., Ong, J.L.: In vitro anti-bacterial and biological properties of magnetron co-sputtered silver-containing hydroxyapatite coating. *Biomater.* **27**, 5512–5517 (2006)
- Dobzyniak, M., Fehring, T.K., Odum, S.: Early failure in total hip arthroplasty. *Clin. Orthop. Relat. Res.* **447**, 76–78 (2006)
- Losina, E., Barrett, J., Mahomed, N.N., Baron, J.A., Katz, J.N.: Early failures of total hip replacement: effect of surgeon volume. *Arthritis Rheum.* **50**, 1338–1343 (2004)
- Long, M., Rack, H.J.: Titanium alloys in total joint replacement—a materials science perspective. *Biomater.* **19**, 1621–1639 (1998)
- Xu, S., Xiaoyu, Y., Yuan, S., Minhua, T., Jian, L., Aidi, N., Xing, L.: Morphology improvement of sandblasted and acid-etched titanium surface and osteoblast attachment promotion by hydroxyapatite coating. *Rare Metal Mater. Eng.* **44**, 67–72 (2015)
- Fujibayashi, S., Neo, M., Kim, H.M., Kokubo, T., Nakamura, T.: Osteoinduction of porous bioactive titanium metal. *Biomater.* **25**, 443–450 (2004)
- Kokubo, T., Yamaguchi, S.: Novel bioactive materials developed by simulated body fluid evaluation: surface-modified Ti metal and its alloys. *Acta Biomater.* **44**, 16–30 (2016)
- Liu, X., Chu, P.K., Ding, C.: Surface modification of titanium, titanium alloys, and related materials for biomedical applications. *Mater. Sci. Eng. R. Rep.* **47**, 49–121 (2004)
- Liu, Y., Jiang, T., Zhou, Y., Zhang, Z., Wang, Z., Tong, H., Shen, X., Wang, Y.: Evaluation of the attachment, proliferation, and differentiation of osteoblast on a calcium carbonate coating on titanium surface. *Mater. Sci. Eng. C.* **31**, 1055–1061 (2011)
- Yanovska, A., Kuznetsov, V., Stanislavov, A., Danilchenko, S., Sukhodub, L.: Synthesis and characterization of hydroxyapatite-based coatings for medical implants obtained on chemically modified Ti6Al4V substrates. *Surf. Coat. Technol.* **205**, 5324–5329 (2011)
- An, S.H., Matsumoto, T., Miyajima, H., Sasaki, J.I., Narayanan, R., Kim, K.H.: Surface characterization of alkali- and heat-treated Ti with or without prior acid etching. *Appl. Surf. Sci.* **258**, 4377–4382 (2012)
- Chen, J.C., Ko, C.L., Lin, D.J., Wu, H.Y., Hung, C.C., Chen, W.C.: In vivo studies of titanium implant surface treatment by sandblasted, acid-etched and further anchored with ceramic of tetracalcium phosphate on osseointegration. *J. Aust. Ceram. Soc.* (2019). <https://doi.org/10.1007/s41779-018-00292-5>
- Deng, F., Zhang, W., Zhang, P., Liu, C., Ling, J.: Improvement in the morphology of micro-arc oxidised titanium surfaces: a new process to increase osteoblast response. *Mater. Sci. Eng. C.* **30**, 141–147 (2010)
- Ban, S., Iwaya, Y., Kono, H., Sato, H.: Surface modification of titanium by etching in concentrated sulfuric acid. *Dent. Mater.* **22**, 1115–1120 (2006)
- Turk, S., Altınsoy, I., Çelebi, G.E., Ipek, M., Ozacar, M., Bindal, C.: A comparison of pretreatments on hydroxyapatite formation on Ti by biomimetic method. *J. Aust. Ceram. Soc.* **54**, 533–543 (2018)
- Kokubo, T., Takadama, H.: How useful is SBF in predicting in vivo bone bioactivity? *Biomater.* **27**, 2907–2915 (2006)
- Ohtsu, N., Kakuchi, Y., Ohtsuki, T.: Antibacterial effect of zinc oxide/hydroxyapatite coatings prepared by chemical solution deposition. *Appl. Surf. Sci.* **445**, 596–600 (2017)
- Yang, A., Han, Y., Pan, Y., Xing, H., Li, J.: Optimum surface roughness prediction for titanium alloy by adopting response surface methodology. *Results Phys.* **7**, 1046–1050 (2017)
- Henriques, B., Sampaio, M., Buciumeanu, M., Souza, J.C.M., Gomes, J.R., Silva, F., Carvalho, O.: Laser surface structuring of Ti6Al4V substrates for adhesion enhancement in Ti6Al4V-PEEK joints. *Mater. Sci. Eng. C.* **79**, 177–184 (2017)
- Baek, S.M., Polyakov, A.V., Moon, J.H., Semenova, I.P., Valiev, R.Z., Kim, H.S.: Effect of surface etching on the tensile behavior of coarse- and ultrafine-grained pure titanium. *Mater. Sci. Eng. A.* **707**, 337–343 (2017)
- Hatamleh, M.M., Wu, X., Alnazzawi, A., Watson, J., Watts, D.: Surface characteristics and biocompatibility of cranioplasty titanium implants following different surface treatments. *Dent. Mater.* **34**, 676–683 (2018)
- Li, B., Li, J., Liang, C., Li, H., Guo, L., Liu, S., Wang, H.: Surface roughness and hydrophilicity of titanium after anodic oxidation. *Rare Metal Mater. Eng.* **45**, 858–862 (2016)
- Shokri, B., Firouzjah, M.A., Hosseini, S.I.: FTIR analysis of silicon dioxide thin film deposited by metal organic-based PECVD. *Proc. 19th Int. Plasma Chem Soc.*, pp. 1–4 (2009)
- Givan, A., Grothe, H., Loewenschuss, A., Nielsen, C.J.: Infrared spectra and ab initio calculations of matrix isolated dimethyl sulfone and its water complex. *Phys. Chem. Chem. Phys.* **4**, 255–263 (2002)
- Hamadani, M., Reisi-Vanani, A., Majedi, A.: Sol-gel preparation and characterization of co/TiO_2 nanoparticles: application to the degradation of methyl orange. *J. Iran. Chem. Soc.* **7**, 52–58 (2010)
- Infrared Spectroscopy Absorption Table-Chemistry LibreTexts. https://chem.libretexts.org/Reference/Reference_Tables/

- [Spectroscopic Parameters/Infrared Spectroscopy Absorption Table](#). Accessed 17 March 2018
27. Yilmaz, B., Evis, Z., Güldiken, M.: Titanyum Alaşımının Biyomimetik Yöntemle Kalsiyum Fosfat Kaplanması. *J. Fac. Eng. Archit. Gazi Univ.* **29**, 105–109 (2014)
 28. Teker, D., Muhaffel, F., Menekse, M., Karaguler, N.G., Baydogan, M., Cimenoglu, H.: Characteristics of multi-layer coating formed on commercially pure titanium for biomedical applications. *Mater. Sci. Eng. C.* **48**, 579–585 (2015)
 29. Liu, D.M., Troczynski, T., Tseng, W.J.: Water-based sol-gel synthesis of hydroxyapatite: process development. *Biomater.* **22**, 1721–1730 (2001)
 30. Avcı, M., Yilmaz, B., Tezcaner, A., Evis, Z.: Strontium doped hydroxyapatite biomimetic coatings on Ti6Al4V plates. *Ceram. Int.* **43**, 9431–9436 (2017)
 31. Silva, C.C., Pinheiro, A.G., Miranda, M.A.R., Góes, J.C., Sombra, A.S.B.: Structural properties of hydroxyapatite obtained by mechanosynthesis. *Solid State Sci.* **5**, 553–558 (2003)
 32. Pylypchuk, I.V., Gorbyk, P.P., Petranovska, A.L., Korduban, O.M., Markovsky, P.E., Ivasyshyn, O.M.: Chapter 7 - Formation of Biomimetic Hydroxyapatite Coatings on the Surface of Titanium and Ti-Containing Alloys: Ti-6Al-4V and Ti-Zr-Nb. *Appl. Nanobiomater.* **3**, 193–229 (2016)
 33. Durdu, S., Usta, M., Berkem, A.S.: Bioactive coatings on Ti6Al4V alloy formed by plasma electrolytic oxidation. *Surf. Coat. Technol.* **301**, 85–93 (2016)
 34. Al-Hazmi, F.E.: Synthesis and electrical properties of Bi doped hydroxyapatite ceramics. *J. Alloys Compd.* **665**, 119–123 (2016)
 35. Wang, H.Y., Zhu, R.F., Lu, Y.P., Xiao, G.Y., He, K., Yuan, Y.F., Ma, X.N., Li, Y.: Effect of sandblasting intensity on microstructures and properties of pure titanium micro-arc oxidation coatings in an optimized composite technique. *Appl. Surf. Sci.* **292**, 204–212 (2014)
 36. Sumathi, S., Buvanewari, G.: Synthesis of apatite structure based $\text{BiNaCa}_3(\text{PO}_4)_3\text{OH}$ and its application for condensation reaction. *Ceram. Int.* **38**, 3547–3552 (2012)
 37. Cochis, A., Azzimonti, B., Valle, C.D., De Giglio, E., Bloise, N., Visai, L., Cometa, S., Rimondini, L., Chiesa, R.: The effect of silver or gallium doped titanium against the multidrug resistant *Acinetobacter baumannii*. *Biomater.* **80**, 80–95 (2016)
 38. Forsgren, J., Svahn, F., Jamar, T., Engqvist, H.: Formation and adhesion of biomimetic hydroxyapatite deposited on titanium substrates. *Acta Biomater.* **3**, 980–984 (2007)
 39. Yilmaz, B., Evis, Z., Tezcaner, A., Banerjee, S.: Surface characterization and biocompatibility of selenium-doped hydroxyapatite coating on titanium alloy. *Int. J. Appl. Ceram. Technol.* **13**, 1059–1068 (2016)
 40. Andrukhov, O., Huber, R., Shi, B., Berner, S., Rausch-Fan, X., Moritz, A., Spencer, N.D., Schedle, A.: Proliferation, behavior, and differentiation of osteoblasts on surfaces of different microroughness. *Dent. Mater.* **32**, 1374–1384 (2016)
 41. Rupp, F., Liang, L., Geis-Gerstorfer, J., Scheideler, L., Hüttig, F.: Surface characteristics of dental implants: a review. *Dent. Mater.* **34**, 40–57 (2018)
 42. Yilmaz, B., Alshemary, A.Z., Evis, Z.: Co-doped hydroxyapatites as potential materials for biomedical applications. *Microchem. J.* **144**, 443–453 (2019)

Publisher's note Springer Nature remains neutral with regard to jurisdictional claims in published maps and institutional affiliations.